

A fused CNN-LSTM model using FFT with application to real-time power quality disturbances recognition

Senfeng Cen¹  | Dong Ok Kim² | Chang Gyoong Lim¹ 

¹Department of Computer Engineering,
Chonnam National University, Yeosu,
South Korea

²National Innovation Cluster Support
Center, Jeonnam Technopark, Suncheon,
Jeonnam, South Korea

Correspondence

Chang Gyoong Lim, Department of
Computer Engineering, Chonnam
National University, Yeosu 59626, South
Korea.

Email: cglim@jnu.ac.kr

Dong Ok Kim, National Innovation
Cluster Support Center, Jeonnam
Technopark, Suncheon, Jeonnam 58034,
South Korea.

Email: dongok7@jntp.or.kr

Funding information

National Innovation Cluster R&D
program, Grant/Award Number:
P0016223

Abstract

With the progress of renewable energy generation and energy storage technologies, more and more renewable sources and devices are integrated into the power system. Due to the complexity of the power system, single and multiple power quality disturbances (PQDs) occur more frequently. Hence, real-time detection of PQDs is the primary issue to mitigate the risk of distortions. This study presents the real-time PQDs classification using fused convolutional neural networks (CNN) combined with long short-term memory (fused CNN-LSTM) architecture based on time and frequency domain features. The frequency-domain features were obtained from time-series data using fast Fourier transform. The original time-domain and frequency-domain features are extracted by respective CNN-LSTM structures. The extracted time and frequency domain features are concatenated to classify the PQD through fully connected layers. Our proposed method was trained and tested using 16 types of synthetic noise PQDs data generated by mathematical models, in accordance with the standard IEEE-1159. Moreover, to further verify the performance of our approach, a simulation distributed power system is carried out to detect various PQDs. We compared three advanced neural network approaches: Deep CNN, CNN-LSTM, and multifusion CNN (MFCNN). The fused CNN-LSTM model takes only 0.64 ms to classify each PQDs signal and achieves an accuracy of 98.95% and 98.89% in synthetic data and simulated power systems which indicates our proposed method outperformed compared methods.

KEY WORDS

convolutional neural network, deep learning, disturbances classification, long short-term memory, power quality disturbances

This is an open access article under the terms of the Creative Commons Attribution License, which permits use, distribution and reproduction in any medium, provided the original work is properly cited.

© 2023 The Authors. *Energy Science & Engineering* published by the Society of Chemical Industry and John Wiley & Sons Ltd.

1 | INTRODUCTION

In recent decades, the demand for energy supply has been increasing explosively in domestic, industrial and commercial, and so forth. However, traditional power generation causes large greenhouse gas emissions, such as oil, coal, and natural gas, which are against sustainable development. Hence, renewable energy (RE) resources have gained attention for reducing environmental effects which generate energy without carbon emissions. The penetration of renewable power generation is increasing gradually with the declining costs of devices and the advancement of technology.¹ The intermittent, fluctuation, and randomness characteristics of most RE (e.g., solar and wind) affect power system stabilization.² With the extensive use of RE sources, nonlinear loads, and other sensitive devices, power quality disturbances (PQDs) occur more frequently. Moreover, the application of bidirectional charging technology, such as vehicle-to-grid and building-to-grid, will lead to more frequent and complex power quality (PQ) issues.³

The term PQDs means that the deviations in voltage, current waveform, or frequency differentiate from the standard. Poor PQ may cause severe hazards, affect power generation, damage sensitive equipment, misoperate the protection device, or even cause power outage. The standard IEEE-1159 characterizes the major categories of PQDs⁴: sag, swell, interruption, harmonics, flicker, notch, spike, and so forth. Considering the potential risks of different PQDs on the power system, real-time

detection and classifying of the PQDs types are the first priority to improve the PQ. Normally, PQDs manifest as complex disturbances rather than single disturbances, which means that multiple disturbances occur simultaneously, especially in distributed energy resource systems.⁵ The presence of multiple disturbances increases the PQDs types, potentially reducing classification accuracy.

Generally, PQDs classification methods are divided into two categories: model-based and data-driven approaches.⁶ The model-based methods are developed based on a deep understanding of the power system and the PQDs definition, the classification accuracy relies on the engineer's domain experience and knowledge.⁷ The distributed energy system increases the difficulty of developing the model-based method due to its complex system topology in distributed power systems. However, data-driven methods allow the model to learn from sufficient data, which does not require domain and detailed energy system knowledge. Figure 1 represents the typical distributed energy system, where distributed RE replaced central power generation. With the implementation of smart grids, advanced metering infrastructure, and the internet of things technologies, a considerable amount of data are being stored in the cloud database, which enables the development of data-driven methods on the enormous amount of measured data.

Traditional PQDs classification methods comprise three stages: feature extraction, feature selection, and disturbances classification.⁸ For feature extraction, various signal processing techniques were applied to extract

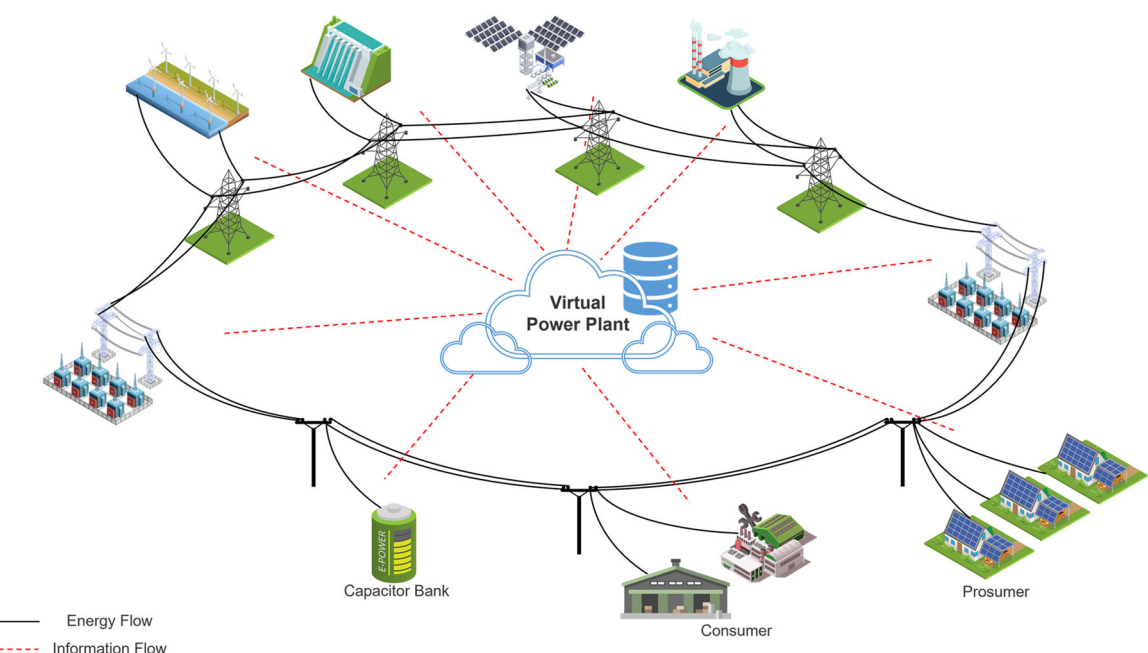


FIGURE 1 The typical distributed energy system.

distinctive features from the original PQDs signal. Xiao et al.⁹ and Borges et al.¹⁰ applied fast Fourier transform (FFT) to extract the frequency domain information for disturbances classification. FFT is an optimized method of discrete Fourier transform (DFT), which is more efficient than DFT, but the results are almost the same.¹¹ Wavelet transform (WT) and its modification were also widely used in PQDs classification, which decomposes the signal into different levels.¹² Kanirajan and Suresh Kumar¹³ adopt 5-level Daubechies 4 (db4) to extract decomposed features. However, the main disadvantages of WT are noise sensitivity and difficulty selecting the appropriate mother wavelet, which may deteriorate the classification accuracy. Hence, several modification methods of the WT are proposed. Kaushik et al.¹⁴ used Hilbert transform and Stockwell transform for feature extraction on 16 types of synthetic PQDs data.

In machine learning, feature selection is an indispensable technique to improve classification performance. Dash et al.¹⁵ used the mean, energy, standard deviation, entropy, skewness, and maximum amplitude statistical features for microgrid disturbances detection. In the study by Borges et al.,¹⁰ the authors extracted 16 statistical features from time and frequency domain data based on the original signal and FFT features. A similar statistical feature selection method from the decomposed wavelet coefficients is presented in Kanirajan and Suresh Kumar.¹³ Liu et al.¹⁶ select the eight eigenvalues from each intrinsic mode function. However, these hand-engineered feature selection methods may remove the critical features. Hence, it is necessary to automatically select the optimal features. An artificial bee colony optimization technique was applied to find the optimal features in Khokhar et al.¹⁷ Ahila et al.¹⁸ applied particle swarm optimization to reduce the redundant features.¹⁸

For disturbances classification, different machine learning algorithms have been proposed to classify the disturbances types. An adaptive K-nearest neighbor method was adopted based on selected features to classify the PQDs in Liu et al.¹⁶ Dash et al.¹⁹ implemented the support vector machine to recognize the single and multiple PQDs based on the tuned features obtained by using whale optimization algorithm. Markovska et al.²⁰ applied random forest to identify the 21 types of PQDs under the different noise level environments based on the hand-engineered feature selection method and verified via LabVIEW. Due to the limitation of selected features, more researchers have proposed diverse deep learning (DL) structures to recognize the different disturbance patterns, which can automatically extract features through hidden layers. A large number of studies based on convolutional neural networks (CNNs) have been used to extract features.^{21,22} Wang and Chen²³

proposed a deep one-dimensional (1D) CNN to classify the PQDs and verify the classification performance on the simulation and multi-microgrid systems. Qiu et al.²⁴ presented multifusion CNN (MFCNN) architecture to recognize the PQDs types under various noises, which fuse the raw signal and FFT features. However, the data type of PQDs is time-series, and CNN structure is commonly used for spatial data.²⁵ Hence, many researchers have used recurrent neural network (RNN) architectures for disturbances classification. Gu et al.²⁶ proposed a new label-guided attention network to classify PQDs types. It comprises the convolutional layers, attention mechanism, and bidirectional RNN. An Enhanced LSTM network method was presented to classify the six events using active power.²⁷ Xiao and Li⁹ proposed an integrated DL method consisting of CNN-GRU, ResNet-GRU, and Inception-GRU networks to identify PQDs.⁹ Moreover, Sindi et al.²⁸ proposed a hybrid convolutional network to identify the disturbance, which combined 1D and 2D features from the original PQDs signal and PQDs image. To address the real-time PQDs classification, we proposed a DL structure named Fused CNN-LSTM, which incorporates CNN and LSTM structures to explore disturbances types. The main contributions of this paper are summarized as follows:

1. Most studies train the model with nonphase shift data which cannot conduct real-time PQDs detection. Our synthetic data contains the different phase shifts that could prevent model overfitting. Considering the periodicity of the PQ waveform and the limitations of the time series signal, to identify and classify complex PQDs more accurately, we adopt the FFT for the time series signal to obtain the frequency domain features.
2. A fused CNN-LSTM architecture is proposed in this paper for PQDs classification, which contains two CNN-LSTM submodules. Compared with the general CNN structure, our two CNN-LSTM submodules individually process the raw PQDs signal and frequency domain features based on FFT. The processed features are concatenated into one layer after CNN-LSTM to recognize the PQDs type.
3. To verify the performance of our fused CNN-LSTM method, we compared the different neural network architectures, including deep CNN, CNN-LSTM, and MFCNN. In addition, a simulation distributed power system is built to simulate the PQDs. It presents the best performance in both synthetic data and simulated environments.

The rest of this article is structured as follows: Section 2 depicts the PQD types and generates the

synthetic data based on the mathematical models. Section 3 describes the architecture of the fused CNN-LSTM model and the implementation process. In Section 4, the experiments and comparisons with other methods are reported. Section 5 presents the results performed under the simulated distributed system environment. Finally, the conclusion and future works are presented in Section 6.

2 | SYNTHETIC DATA GENERATION

To support the validity of our proposed model, efficient PQDs data is required, which includes various disturbances. IEEE-1159 defines different PQDs types and their parameter variations.⁴ In this work, the 16 types of single and multiple synthetic PQDs signals are generated in Python according to the mathematical model. The PQDs mathematical models are shown in Tables 1 and 2, which contain 10 single types and 6 multiple types. In PQDs mathematical equations, the symbol A, normally equal to 1 is a constant value that represents the waveform amplitude. The α in the equations describe the various intensity of disturbances in different events. $u(t)$ is a step function that could control the duration of the disturbances. For example, $u(t - t_1) - u(t - t_2)$ in the equation means the disturbances occurred during t_1 to t_2 . The sign function $\text{sgn}()$ is a real-valued step function that can be defined as:

$$\text{sgn}(x) = \begin{cases} 1, & \text{if } x > 0 \\ 0, & \text{if } x = 0 \\ -1, & \text{if } x < 0 \end{cases} \quad (1)$$

One thousand waveforms are generated in each disturbance type by randomly changing the parameter values. It records the 10 cycles signal in each PQDs waveform. The fundamental frequency and sampling rate are set to 50 Hz and 10 kHz, respectively. According to the above conditions, each waveform records data every 0.2 s, containing 2000 sample points. The single and multiple PQDs waveforms are shown in Figures 2 and 3. A total of 16,000 PQDs data is split into training, validation, and test sets in the ratio of 6:2:2. However, the real PQDs data was collected from sensors that usually contain noise.²⁹ Hence, different levels of Gaussian white noise are added to the training and validation set to improve the accuracy of our proposed model.^{30,31} In the test set, the signal-to-noise ratio with 20, 30, and 40 dB are added to the test set, respectively. A brief description of each dataset is shown in Table 3.

3 | PROPOSED PQDS CLASSIFICATION METHODOLOGY

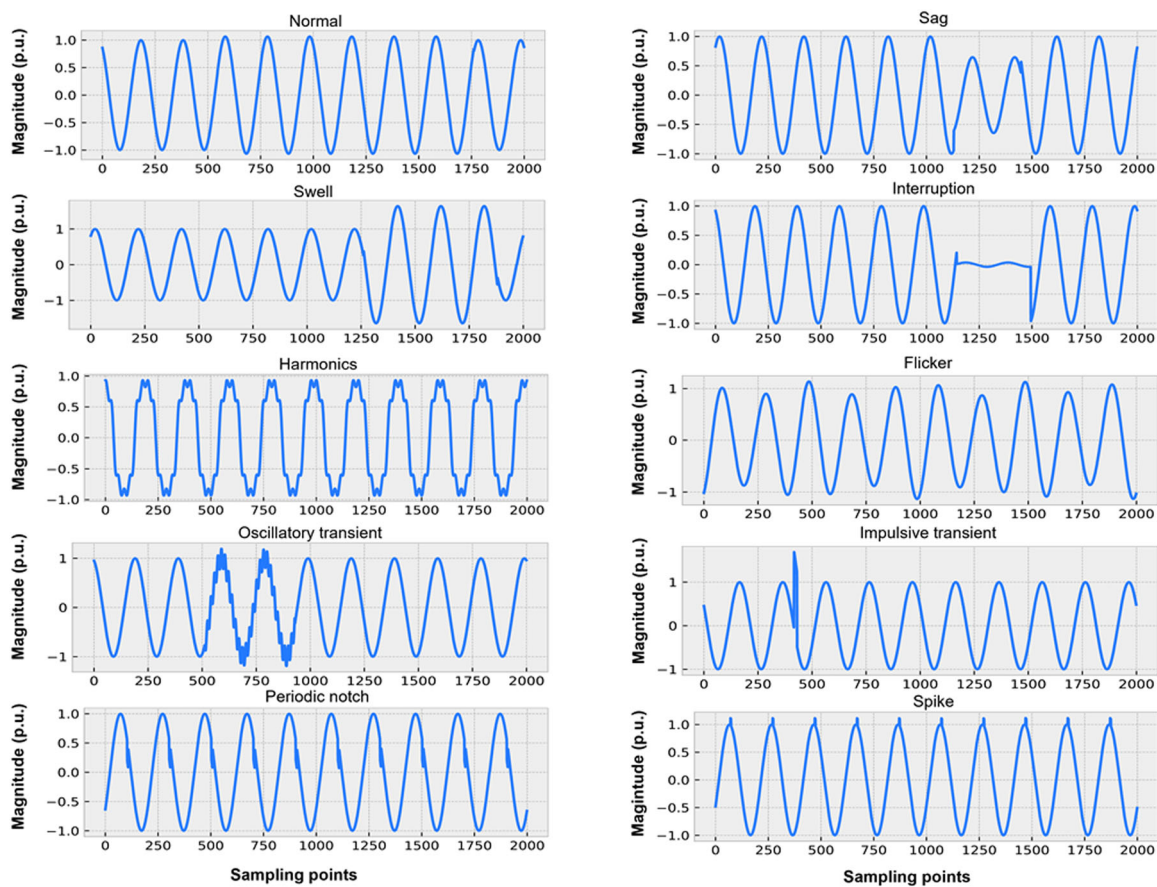
This section introduced our proposed fused CNN-LSTM architecture, which fused time and frequency features based on the time and frequency domain inputs for PQDs

TABLE 1 Mathematical models of single power quality disturbances.

Disturbances	Mathematical equation	Parameters
Normal (C1)	$y(t) = A[1 \pm \alpha(u(t - t_1) - u(t - t_2))] \sin(\omega t)$	$\alpha < 0.1, T \leq t_2 - t_1 \leq 9T$
Sag (C2)	$y(t) = A[1 - \alpha(u(t - t_1) - u(t - t_2))] \sin(\omega t)$	$0.1 \leq \alpha \leq 0.9, T \leq t_2 - t_1 \leq 9T$
Swell (C3)	$y(t) = A[1 + \alpha(u(t - t_1) - u(t - t_2))] \sin(\omega t)$	$0.1 \leq \alpha \leq 0.8, T \leq t_2 - t_1 \leq 9T$
Interruption (C4)	$y(t) = A[1 - \alpha(u(t - t_1) - u(t - t_2))] \sin(\omega t)$	$0.9 \leq \alpha \leq 1, T \leq t_2 - t_1 \leq 9T$
Harmonics (C5)	$y(t) = A[\alpha_1 \sin(\omega t) + \alpha_3 \sin(3\omega t) + \alpha_5 \sin(5\omega t) + \alpha_7 \sin(7\omega t)]$	$0.05 \leq \alpha_3, \alpha_5, \alpha_7 \leq 0.15, \sum(\alpha_i)^2 = 1$
Flicker (C6)	$y(t) = A[1 + \alpha_f \sin(\beta\omega t)] \sin(\omega t)$	$0.1 \leq \alpha_f \leq 0.2, 5 \leq \beta \leq 20\text{Hz}$
Impulsive transient (C7)	$y(t) = A \left[\sin(\omega t) + \alpha \exp\left(-\frac{t-t_1}{\tau}\right) ((u(t - t_1) - u(t - t_2))) \right]$	$0.1 \leq \alpha \leq 0.8, T/20 \leq t_2 - t_1 \leq T/10, 8 \leq \tau \leq 40$
Oscillatory transient (C8)	$y(t) = A \left[\sin(\omega t) + \alpha \exp\left(-\frac{t-t_1}{\tau}\right) \sin \omega_n(t - t_1) \cdot (u(t - t_1) - u(t - t_2)) \right]$	$0.1 \leq \alpha \leq 0.8, 0.5T \leq t_2 - t_1 \leq 3T, 8 \leq \tau \leq 40, 300 \leq f_n \leq 900\text{Hz}$
Periodic notch (C9)	$y(t) = \sin(\omega t) - \text{sgn}(\sin(\omega t)) \times \{\sum_0^9 k [u(t - (t_1 - 0.02n)) - u(t - (t_2 - 0.02n))]\}$	$0 \leq t_1, t_2 \leq 0.5T, 0.01T \leq t_2 - t_1 \leq 0.05T, 0.1 \leq k \leq 0.4$
Spike (C10)	$y(t) = \sin(\omega t) + \text{sgn}(\sin(\omega t)) \times \{\sum_0^9 k [u(t - (t_1 - 0.02n)) - u(t - (t_2 - 0.02n))]\}$	$0 \leq t_1, t_2 \leq 0.5T, 0.01T \leq t_2 - t_1 \leq 0.05T, 0.1 \leq k \leq 0.4$

TABLE 2 Mathematical models of multiple power quality disturbances.

Disturbances	Mathematical equation	Parameters
Sag with harmonics (C11)	$y(t) = A[1 - \alpha(u(t - t_1) - u(t - t_2))][\alpha_1 \sin(\omega t) + \alpha_3 \sin(3\omega t) + \alpha_5 \sin(5\omega t) + \alpha_7 \sin(7\omega t)]$	$0.1 \leq \alpha \leq 0.9, T \leq t_2 - t_1 \leq 9T$ $0.05 \leq \alpha_3, \alpha_5, \alpha_7 \leq 0.15, \sum(\alpha_i)^2 = 1$
Swell with harmonics (C12)	$y(t) = A[1 + (u(t - t_1) - u(t - t_2))][\alpha_1 \sin(\omega t) + \alpha_3 \sin(3\omega t) + \alpha_5 \sin(5\omega t) + \alpha_7 \sin(7\omega t)]$	$0.1 \leq \alpha \leq 0.8, T \leq t_2 - t_1 \leq 9T$ $0.05 \leq \alpha_3, \alpha_5, \alpha_7 \leq 0.15, \sum(\alpha_i)^2 = 1$
Interruption with harmonics (C13)	$y(t) = A[1 - \alpha(u(t - t_1) - u(t - t_2))][\alpha_1 \sin(\omega t) + \alpha_3 \sin(3\omega t) + \alpha_5 \sin(5\omega t) + \alpha_7 \sin(7\omega t)]$	$0.9 \leq \alpha \leq 1, T \leq t_2 - t_1 \leq 9T$ $0.05 \leq \alpha_3, \alpha_5, \alpha_7 \leq 0.15, \sum(\alpha_i)^2 = 1$
Flicker with harmonics (C14)	$y(t) = A[1 + \alpha_f \sin(\beta\omega t)][\alpha_1 \sin(\omega t) + \alpha_3 \sin(3\omega t) + \alpha_5 \sin(5\omega t) + \alpha_7 \sin(7\omega t)]$	$0.1 \leq \alpha_f \leq 0.2, 5 \leq \beta \leq 20Hz$ $0.05 \leq \alpha_3, \alpha_5, \alpha_7 \leq 0.15, \sum(\alpha_i)^2 = 1$
Flicker with sag (C15)	$y(t) = A[1 + \alpha_f \sin(\beta\omega t)][1 - \alpha(u(t - t_1) - u(t - t_2))]\sin(\omega t)$	$0.1 \leq \alpha_f \leq 0.2, 5 \leq \beta \leq 20Hz$ $0.1 \leq \alpha \leq 0.9, T \leq t_2 - t_1 \leq 9T$
Flicker with swell (C16)	$y(t) = A[1 + \alpha_f \sin(\beta\omega t)][1 + \alpha(u(t - t_1) - u(t - t_2))]\sin(\omega t)$	$0.1 \leq \alpha_f \leq 0.2, 5 \leq \beta \leq 20Hz$ $0.1 \leq \alpha \leq 0.9, T \leq t_2 - t_1 \leq 9T$

**FIGURE 2** Single power quality disturbances waveforms.

classification. As mentioned in Section 2, the PQDs data are time-series signals in 10 cycles which contains 2000 sampling points. In addition, the frequency domain input data were obtained by FFT. Our proposed method

consists of three main phases. The first phase is to obtain the frequency domain information, which employs FFT to transform the time-series data. Subsequently, the Z-score normalization method is applied to rescale the

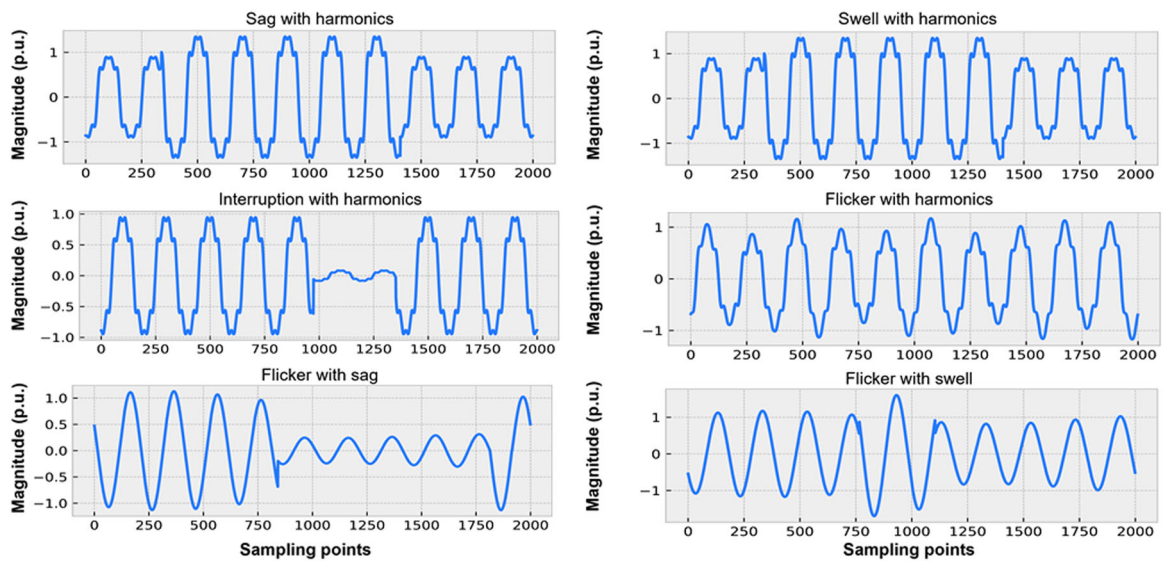


FIGURE 3 Multiple power quality disturbances waveforms.

TABLE 3 Generated synthetic data for the proposed method.

Dataset	Number	Noise level
Training set	$16 \times 600 = 9600$	From 20 to 40 dB
Validation set	$16 \times 200 = 3200$	From 20 to 40 dB
Test set 1	$16 \times 200 = 3200$	Pure
Test set 2	$16 \times 200 = 3200$	20 dB
Test set 3	$16 \times 200 = 3200$	30 dB
Test set 4	$16 \times 200 = 3200$	40 dB

time and frequency domain features based on standard deviation and mean. Finally, the fused CNN-LSTM architecture is proposed to merge the time and frequency features from the two CNN-LSTM submodules for disturbances classification.

Given a set of N PQDs signals $X_t = \{x_{1t}, x_{2t}, \dots, x_{Nt}\}$ where $x_{it} = \langle x_{it1}, x_{it2}, \dots, x_{itn} \rangle$ and n represents the time domain features in each PQDs waveform. The purpose of our study is to correctly classify the disturbances type $C = \{c_1, c_2, \dots, c_k\}$. The details of our proposed method are as follows.

3.1 | Fast Fourier transform

The first phase aims to obtain the frequency domain information from PQDs signals. Considering that time-series signals are not appropriate for some types of recognition, especially in the case of harmonics distortions. FFT is adopted to obtain frequency domain information from the PQDs signals, which decompose

the signal into different sinusoid frequencies. The process of FFT can be expressed as follow:

$$X(k) = \sum_{m=0}^{N/2-1} x(2m)W_N^{k(2m)} + \sum_{m=0}^{N/2-1} x(2m+1)W_N^{k(2m+1)}, \quad (2)$$

where $W_n = e^{-j2\pi/N}$ and k is the sampling point from 0 to $N - 1$. After applying FFT, it obtained one frequency output denoted as $X_f = \{x_{1f}, x_{2f}, \dots, x_{Nf}\}$ where $x_{if} = \langle x_{if1}, x_{if2}, \dots, x_{ifm} \rangle$ and m is the frequency features from FFT.

The typical PQDs waveform under noise environment and frequency component plots are illustrated in Figure 4A-D from top to bottom. It can be noted that from each frequency component plot, the fundamental frequency is 50 Hz. The frequency component results in Figure 4B indicate that harmonic components exist in the waveform, which are third, fifth, and seventh, respectively. However, it is difficult to distinguish the detailed harmonic components from the original PQDs waveform.

3.2 | Data normalization

Data Normalization is essential before training the classification model that rescales each feature in the fixed range, such as decimal scaling normalization, min-max normalization, Z-score normalization (ZSN),³² and so forth. In this work, ZSN is applied to the original signal X_t and frequency features X_f .³³ The corresponding

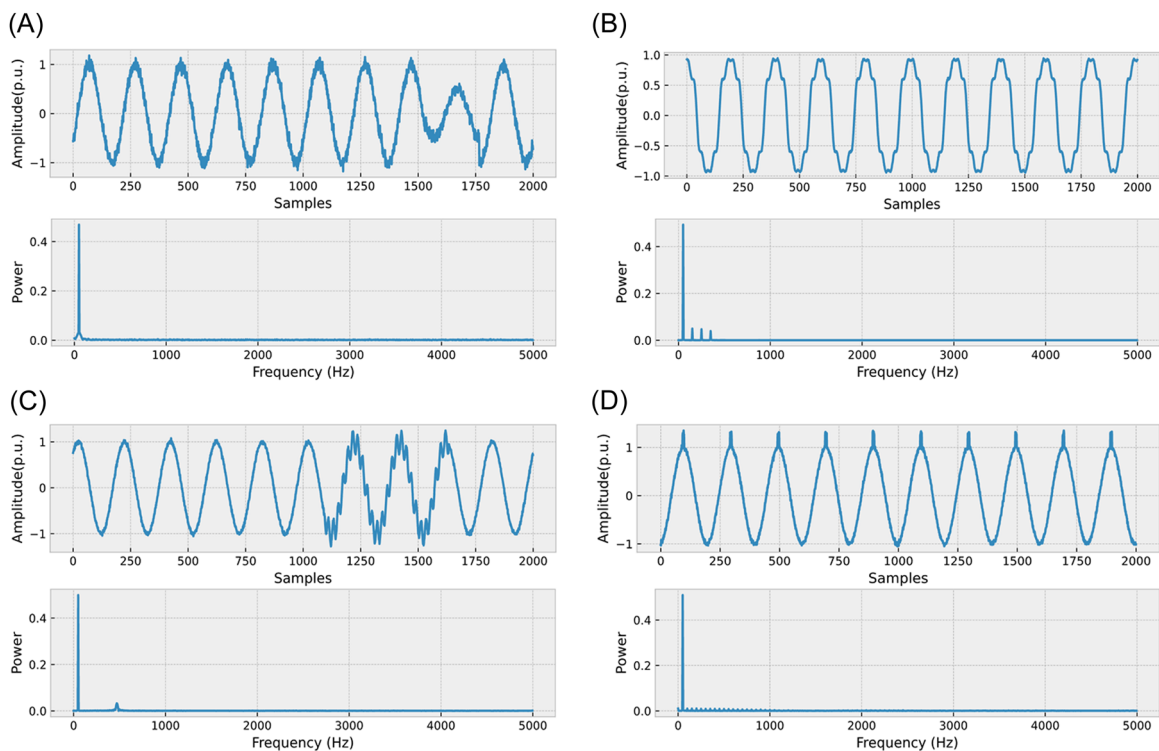


FIGURE 4 PQDs waveform and its frequency component in noisy environments. (A) Sag, (B) harmonics, (C) oscillatory transient, and (D) spike.

normalized time and frequency features are denoted as $x'_{it} = \langle x'_{it1}, x'_{it2}, \dots, x'_{itn} \rangle$ and $x'_{if} = \langle x'_{if1}, x'_{if2}, \dots, x'_{ifm} \rangle$. The calculation of each feature x'_{itn} and x'_{ifm} are as follows:

$$x'_{itn} = \frac{x_{itn} - \mu_{tn}}{\sigma_{tn}}, \quad (3)$$

$$x'_{ifm} = \frac{x_{ifm} - \mu_{fm}}{\sigma_{fm}}, \quad (4)$$

where μ_{tn} , μ_{fm} , and σ_{tn} , σ_{fm} are the mean and standard deviation of i th features in time and frequency domain data, respectively. The mean and standard deviation of each time and frequency data rescaled variable are 0 and 1. Although data normalization avoids the numerical distance between different features, it cannot ensure the existence of irrelevant features. These unwanted features could deteriorate the classification accuracy and increase the computational complexity. Thus, eliminating irrelevant features is necessary for improving classification accuracy.

3.3 | Fused CNN-LSTM model

As normalized time and frequency data individually contain partial features in different PQDs. This study proposes a fused CNN-LSTM model based on time and

frequency domain data for disturbances classification. The CNN and LSTM modules are used to extract spatial and sequential information, respectively. The architecture of our proposed model is shown in Figure 5. Our fused CNN-LSTM framework processes time domain and frequency domain signals separately and simultaneously. It contains three stacked CNN modules denoted as Conv1, Conv2, Conv3, and one LSTM layer. The CNN module consists of two 1D convolutional layers, a max-pooling layer, and batch normalization, which is similar to the VGG network.³⁴ As shown in Figure 5, each convolutional layer uses the same stride, kernel size, and activation function except that the number of filters increases as the depth increases. The LSTM layer is connected after the three stacked CNN modules. The features of two CNN-LSTM modules are concatenated and input to the two fully connected (FC) layers. To ensure the model generalization,³⁵ the dropout ratio is set to 0.2 in FC layers to prevent overfitting. Finally, the softmax activation function in the output layer is used to map the classification probability.

The convolutional layer in CNN is the most significant difference from the conventional neural networks, which extract features based on convolution filters with shared weights and biases. Compared with conventional approaches, CNN decreases the parameters dramatically and achieves good performance by convolutional kernels.

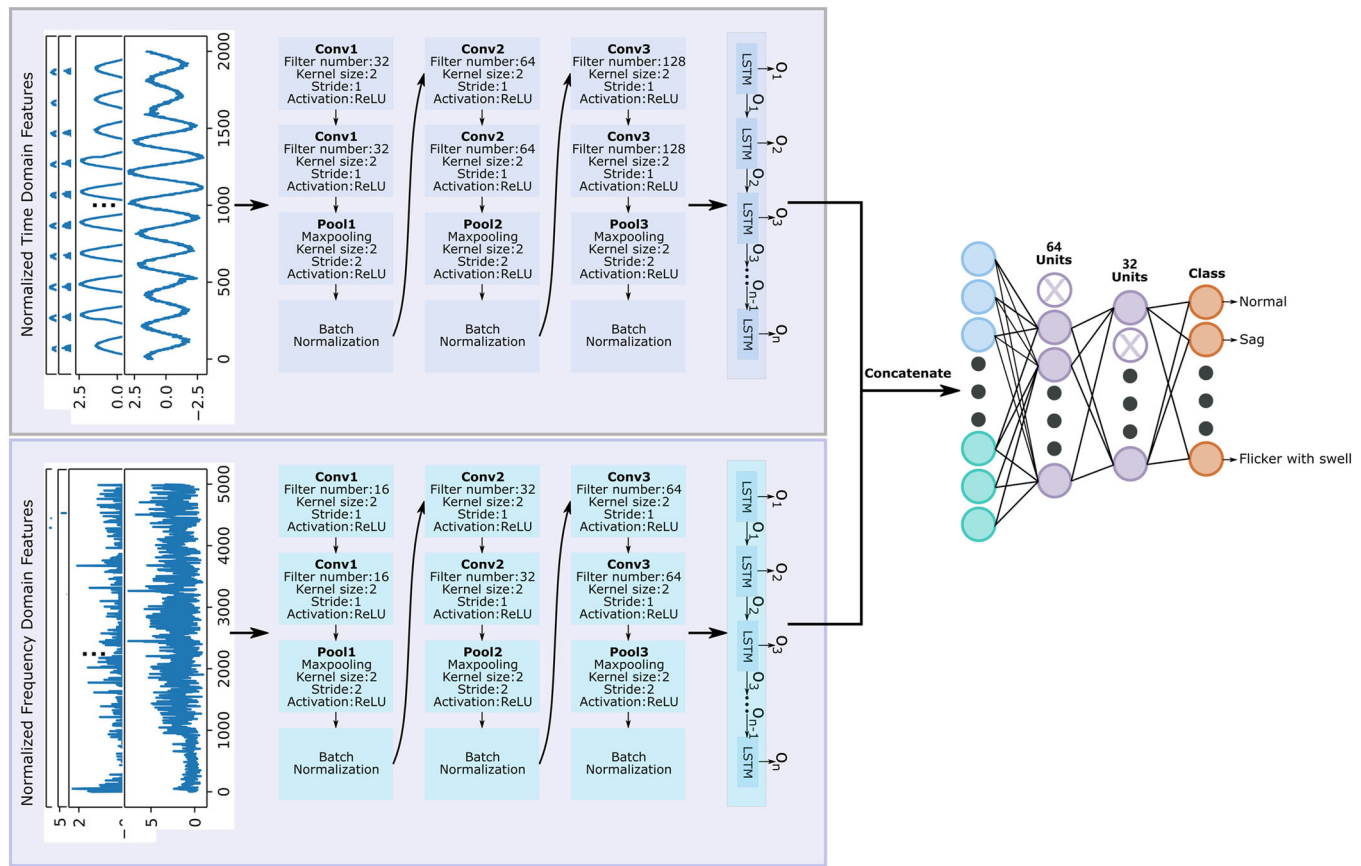


FIGURE 5 The architecture of the fused CNN-LSTM model.

The output of the 1D convolutional layer can be expressed as:

$$X_o^l = \sigma \left(\sum_i X_i^{l-1} \times w_j^l + b^l \right) \quad (5)$$

where X_i^{l-1} is the 1D input in $l-1$ th layer, w_j^l is the filter kernel, b^l represents the bias, and $\sigma(\cdot)$ indicates the activation function. A fixed convolution kernel with the size of 2 and stride of 1 is applied as shown in Figure 5.

The rectified linear units activation function is used after each convolutional layer to add the nonlinearity. Long short-term memory, a variant of RNN architecture, was used to solve sequential data problems, such as machine translation and speech recognition. The unit in LSTM is called “cell”, which is more complicated than traditional neurons. An LSTM cell comprises three parts: the input gate, the output gate, and forget gate. Figure 6 shows the standard LSTM architecture. These sophisticated LSTM cells connect to each other, enabling LSTM to distinguish useful long-term and short-term features. The equations in the LSTM cell can be defined as:

$$i_t = \sigma_s(W_i x_t + U_i h_{t-1} + b_i), \quad (6)$$

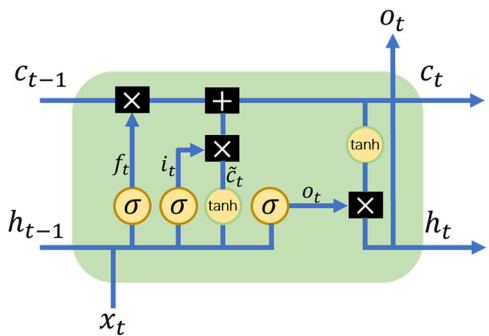


FIGURE 6 The LSTM cell architecture.

$$f_t = \sigma_s(W_f x_t + U_f h_{t-1} + b_f), \quad (7)$$

$$o_t = \sigma_s(W_o x_t + U_o h_{t-1} + b_o), \quad (8)$$

$$\tilde{c}_t = \sigma_{\tanh}(W_c x_t + U_c h_{t-1} + b_c), \quad (9)$$

$$c_t = f_t \odot c_{t-1} + i_t \odot \tilde{c}_t, \quad (10)$$

$$h_t = o_t \odot \sigma_{\tanh}(c_t), \quad (11)$$

where x and h represent the input and hidden state, t and $t-1$ are time steps. i_t , f_t , o_t are the vectors of the input,

forget, and output gate in the LSTM cell. \tilde{c}_t and c_t are the cell input vector and cell state vector. \odot is the element-wise product, σ_s and σ_{tanh} are the activation functions of sigmoid and tanh, respectively. The parameters W_* , U_* , and b_* are the weights and biases in different gates.

4 | EXPERIMENT RESULTS

4.1 | Training and evaluating the model

To verify the effectiveness of the Fused CNN-LSTM, 16 types of synthetic PQDs data, as mentioned in Section 2, are used to train the model. The categorical cross-entropy and Adam optimizer are adopted to train our model. Categorical cross-entropy is a loss function commonly used for classification. It computes the single data loss value between the category label and predictions, and the cost function can be calculated by:

$$CE(\hat{y}, y) = -\frac{1}{N} \frac{1}{C} \sum_{i=1}^N \sum_{j=1}^C [y_{ij} \log \tilde{y}_{ij} + (1 - y_{ij}) \log(1 - \tilde{y}_{ij})], \quad (12)$$

where $y_i = \langle y_{i1}, y_{i2}, \dots, y_{ic} \rangle$ represents the i th signal corresponded label and $\tilde{y}_i = \langle \tilde{y}_{i1}, \tilde{y}_{i2}, \dots, \tilde{y}_{ic} \rangle$ is the predicted score vector for the signal i .

Through several experiment comparisons, the optimal configuration and hyperparameters of our proposed network are presented in Table 4. The batch size is set to 32, which updates the model parameters based on backpropagation by randomly selecting the data from the training set. A total of 70 epochs are used to train the model. The initial learning rate is set to 0.001 and automatically reduced by 1/10 if the loss

TABLE 4 The hyperparameters of the fused CNN-LSTM model.

Hyperparameter	Range
1 CNN filter number	[32, 64, 128] (time domain) [16, 32, 64] (frequency domain)
2 LSTM nodes	[128, 64] (time and frequency domain)
3 Optimizer	Adam
4 Learning rate	[1e-5]
5 Epochs	70
6 Batch size	32
7 Dropout	0.2

value in the validation set does not decrease during 10 epochs. The proposed method is trained and evaluated in the TensorFlow framework based on Python 3.7 environment with an Intel Core Xeon CPU (2.3 GHz), 16 GB DDR4 RAM, and an NVIDIA Tesla P100 GPU.

The detailed results of our method for each type under different noise environments are listed in Table 5. As shown in Table 5, the accuracy under 20, 30, 40 dB, and pure noise environment are 97.75%, 99.34%, 99.37%, and 99.34%, respectively. The high-level noise (20 dB) data accuracy is relatively lower than in low-noise and no-noise environments (30 dB, 40 dB, and pure).

4.2 | Analysis of experimental results with model comparison

To demonstrate the advantages of the fused CNN-LSTM model, we applied three advanced neural network architectures without using handcrafted feature selection methods for comparison. The details of the comparison methods are introduced as follows.

TABLE 5 The detailed performance of the fused CNN-LSTM model.

Disturbances type	Accuracy			
	20 dB	30 dB	40 dB	Pure
Normal	92.5	99.5	100	99
Sag	97	98	99.5	99.5
Swell	99	98.5	98.5	99
Interruption	99.5	100	99.5	99
Harmonics	100	100	100	100
Flicker	100	100	100	100
Impulsive transient	100	100	100	100
Oscillatory transient	99	100	100	100
Periodic notch	89	99	99	99.5
Spike	98	99	99	99
Sag with harmonics	98.5	98.5	98.5	98.5
Swell with harmonics	99.5	100	100	100
Interruption with harmonics	99.5	100	99.5	99.5
Flicker with harmonics	100	100	100	100
Flicker with sag	97	98	97.5	97.5
Flicker with swell	95.5	99	99	99
Average	97.75	99.34	99.37	99.34

4.2.1 | Deep CNN

A deep CNN architecture in the study by Wang and Chen²³ comprises 1D convolutional layers, Max-pooling layers, and dense layers. The kernel size of convolution and Max-pooling layers is 2, and the strides are 1 and 2. The units of three dense layers are 256, 128, and 16, respectively.

4.2.2 | CNN-LSTM

A hybrid architecture was adopted by Mohan et al.³⁶ It contains 64 and 128 filters with stride 3 in two convolutional layers. One LSTM layer with 50 cells is connected to the convolutional layers, and a FC layer is used to represent the PQDs type.

4.2.3 | Multifusion CNN

The MFCNN model²⁴ uses raw PQDs signal and its FFT signal as an input. During convolutional layers, the time and frequency domain features are merged into one layer. Then the combined features are connected with the three dense layers to classify the disturbance types.

Considering the PQDs signal length in our dataset, directly implementing the above models may lead to unsatisfactory results. Thus, to compare the model performance reasonably, we modified some model parameters and configurations based on our experience. The details of the abovementioned models for PQDs classification are shown in Tables 6 and 7.

Figure 7 shows the performances of the abovementioned algorithms after tuning the hyperparameters. It clearly shows that our proposed model outperforms other models under different noise environments. The accuracy of deep CNN and CNN-LSTM is better than MFCNN. The average accuracy of deep CNN and CNN-

TABLE 6 The structures of compared models.

Models	Layers (not including max-pooling layers)
Deep CNN	1D Convolutional layer: 9 Dense layer: 3
CNN-LSTM	1D Convolutional layer: 9 LSTM layer: 1 Dense layer: 1
MFCNN	1D Convolutional layer: 6 Dense layer: 3

TABLE 7 The model comparison of four methods.

Models	Number of parameters	Training time	Model size	Test time (per data)
Fused CNN-LSTM	327,536	16.33 min	6.3 MB	0.64 ms
DCNN	229,392	8.02 min	2.78 MB	0.32 ms
CNN-LSTM	254,228	11.72 min	3.06 MB	0.47 ms
MFCNN	308,528	8.22 min	3.66 MB	0.35 ms

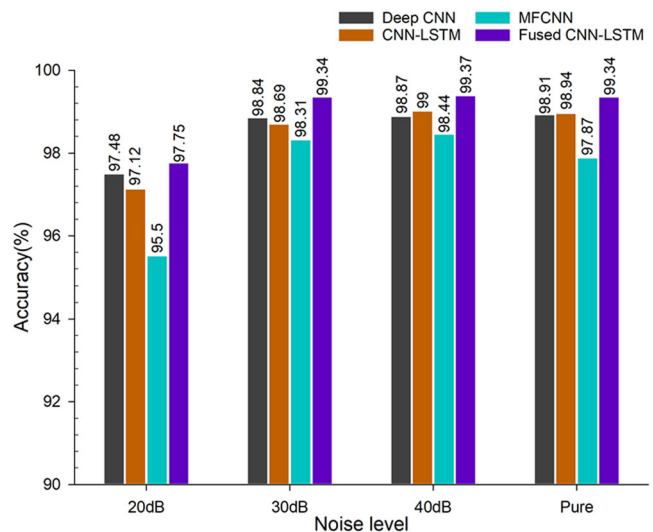


FIGURE 7 The performance of the different models.

LSTM is about 98.5% and MFCNN achieved the lowest result with 97.38%. It can be observed that the performance of the different methods in 30 dB, 40 dB, and pure conditions are similar. However, under the 20 dB noise environment, the accuracy of deep CNN, CNN-LSTM, and fused CNN-LSTM decreased by 1.5%. But MFCNN decreased by more than 2.5% to 95.5%, which is very susceptible to noise.

5 | COMPARISON OF METHODS ON SIMULATED SYSTEM

The proposed method was further validated in the typical distributed system. Figure 8 shows the detailed distributed system, which consists of two wind generators, one photovoltaic generator, one synchronous generator, a high-voltage network, and different load types. The 0.6 kV distribution network is connected to the 115 kV high-voltage network through the step-up transformer. The fundamental and sampling frequency are the same as the synthetic data configuration.

The different types of PQDs signal were obtained by manually creating various faults, special operations, and faults durations, such as line faults, nonlinear loads, and so forth. Considering the voltage signals are monitored and recorded from different voltage level locations, various amplitudes of PQDs were converted into per unit according to its bus voltage. The typical types of PQD voltage waveforms from the simulated system are shown in Figure 9. The three waveforms using different colors in Figure 9A–D represent the three-phase fault

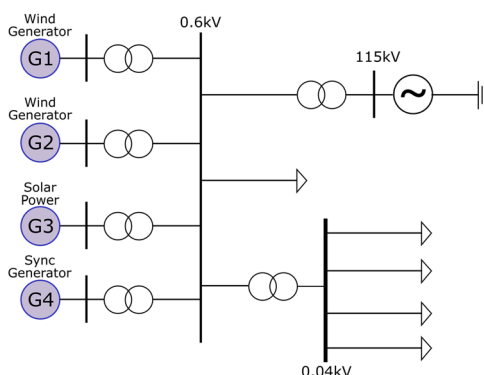


FIGURE 8 The simulated distribution system.

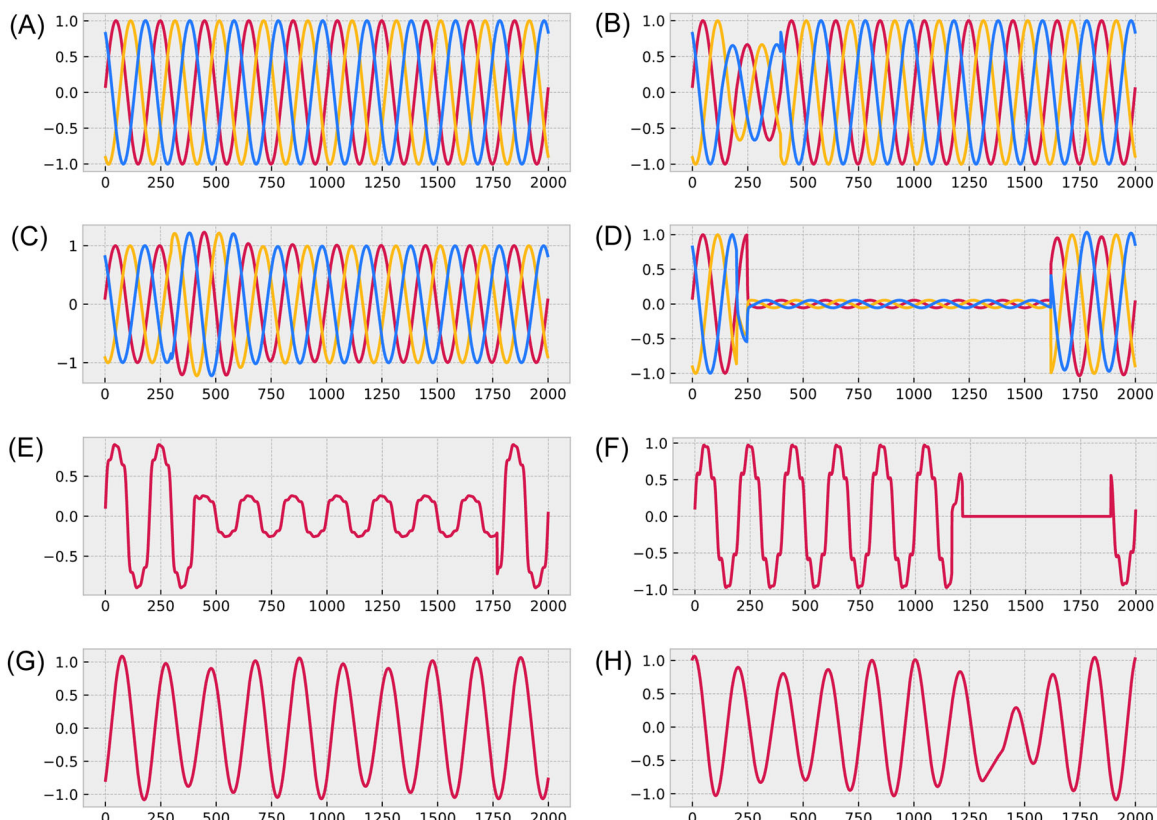


FIGURE 9 Three-phase voltage waveform: (A) normal, (B) sag, (C) swell, (D) interruption, and one-phase voltage waveform: (E) sag with harmonics, (F) interruption with harmonics, (G) flicker, (H) flicker with sag.

waveforms. Figure 9E–H shows the single-phase disturbance waveform.

Table 8 summarizes the disturbances identification results of different methods in simulated data. As shown in Table 8, the average accuracy of fused CNN-LSTM is 98.89%, which is better than deep CNN, CNN-LSTM, and MFCNN. It shows that deep CNN, CNN-LSTM, and MFCNN models can not accurately recognize the flicker disturbances. But our proposed method achieves 90% accuracy on flicker disturbances. The confusion matrix in Figure 10A–D clearly shows the predicted results of four neural network models.

As shown in Figure 10A, the deep CNN model can not accurately identify the flicker and harmonics disturbances. For the 50 signals of the flicker waveform, 40 signals are detected correctly, and 10 are misclassified as flicker with swell disturbance. Among the 100 harmonics signals, only 34 harmonics disturbances are identified correctly. The rest of the harmonics waveforms are classified to flicker with harmonics, oscillatory transient, sag with harmonics and swell with harmonics which means Deep CNN cannot precisely identify the harmonics disturbances. The confusion matrix of CNN-LSTM in Figure 10B shows most PQDs data are classified correctly except for flicker and normal types. From the 50

TABLE 8 The detailed performance of various methods.

Disturbances type	Number	Accuracy (%)			
		DCNN	CNN-LSTM	MFCNN	Fused CNN-LSTM
Normal	150	100	78.67	100	96.67
Sag	150	99.33	99.33	100	100
Swell	150	100	98.67	94	100
Interruption	150	100	100	98.67	100
Harmonics	100	34	96	100	100
Flicker	50	80	70	8	90
Sag with harmonics	100	100	100	100	100
Swell with harmonics	100	94	100	100	100
Interruption with harmonics	100	100	100	100	100
Flicker with sag	35	97.14	97.14	100	94.28
Average		92.26	94.93	94.75	98.89

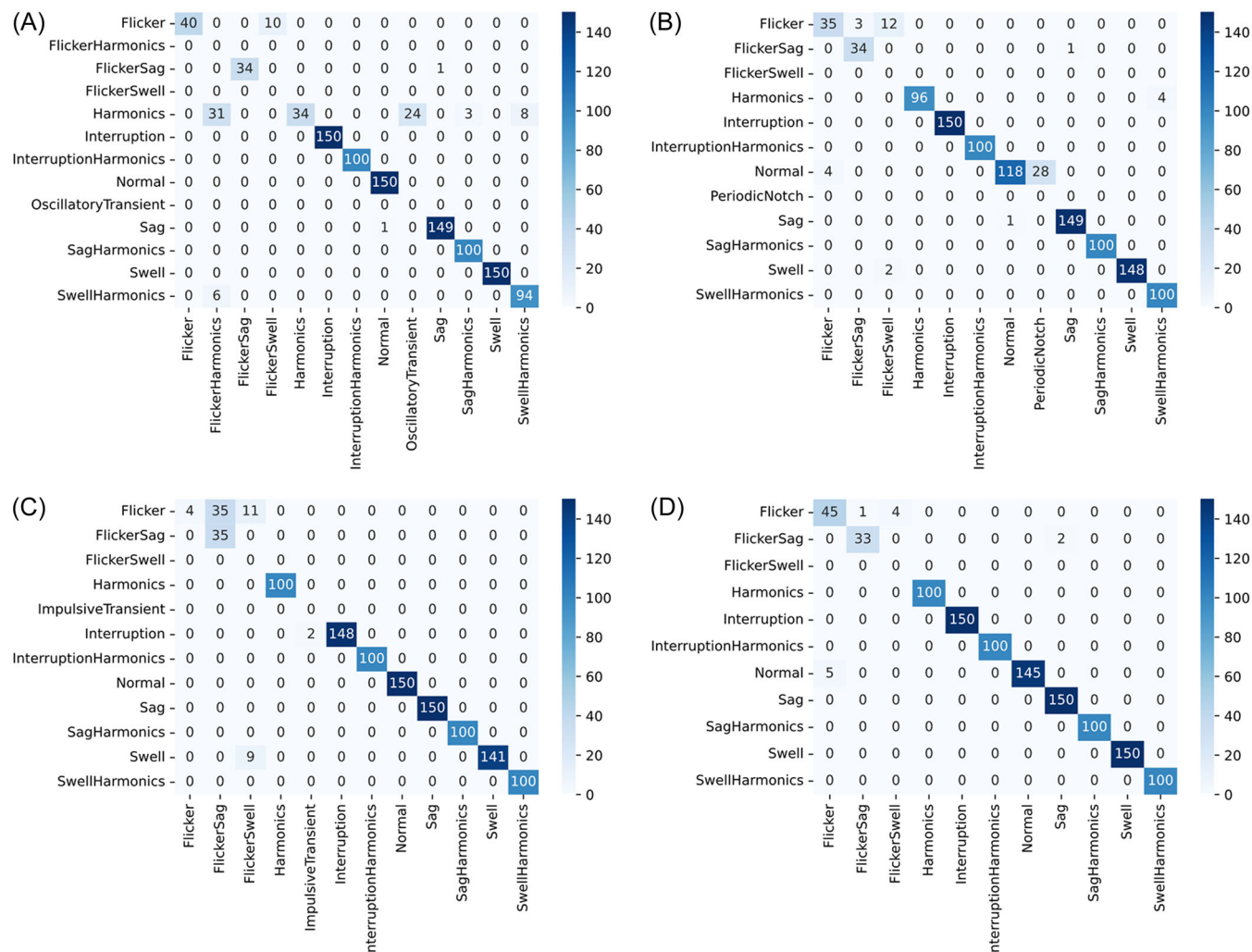


FIGURE 10 The confusion matrix of different methods. (A) Deep CNN, (B) CNN-LSTM, (C) MFCNN, and (D) fused CNN-LSTM.

flicker disturbances, 3 and 12 signals are misclassified to the type of flicker with sag and flicker with swell which are the multiple disturbances of flicker. The 28 normal signals are identified as periodic notch disturbances. Figure 10C shows that the MFCNN model can not distinguish the flicker and its multiple disturbances, only four flicker disturbances are classified correctly. However, the recognition result in Figure 10D demonstrated that our proposed model achieved the best performance.

6 | CONCLUSION

This paper proposes a fused CNN-LSTM to identify the PQDs types using time and frequency domain features. The original PQDs signal and frequency data were processed by CNN-LSTM individually. Afterward, the extracted time and frequency domain features were fused into one layer. Finally, two FC layers and a softmax classifier were used to predict the disturbances category. In particular, the fusion of time and frequency features enhances the accuracy in detecting PQDs. Comparison analysis of classification time consumption and accuracy with other methods in synthetic and simulated data demonstrates that our proposed method is more suitable for applications, including noise environments. Future works will focus on improving the noise environment classification accuracy and adding more complex PQDs types.

ACKNOWLEDGMENTS

This research was supported by Jeollanam-do and financially supported by the Ministry of Trade, Industry and Energy (MOTIE) and Korea Institute for Advancement of Technology (KIAT) under the research project: “National Innovation Cluster R&D program” (Grant number: P0016223).

CONFLICT OF INTEREST STATEMENT

The authors declare no conflict of interest.

ORCID

Senfeng Cen  <http://orcid.org/0000-0002-8635-8112>
 Chang Gyoong Lim  <http://orcid.org/0000-0002-2295-568X>

REFERENCES

- Mohamed MA, Abdullah HM, Al-Sumaiti AS, El-Meligy MA, Sharaf M, Soliman AT. Towards energy management negotiation between distributed AC/DC networks. *IEEE Access*. 2020;8:215438-215456. doi:[10.1109/ACCESS.2020.3040503](https://doi.org/10.1109/ACCESS.2020.3040503)
- Liang X. Emerging power quality challenges due to integration of renewable energy sources. *IEEE Trans Ind Appl*. 2017;53(2):855-866. doi:[10.1109/TIA.2016.2626253](https://doi.org/10.1109/TIA.2016.2626253)
- Balasundar C, Sundarabalan CK, Sharma J, Srinath NS, Guerrero JM. Design of power quality enhanced sustainable bidirectional electric vehicle charging station in distribution grid. *Sustain Cities Soc*. 2021;74:103242. doi:[10.1016/j.scs.2021.103242](https://doi.org/10.1016/j.scs.2021.103242)
- IEEE Recommended Practice for Monitoring Electric Power Quality. IEEE Power and Energy Society. 2009.
- Liu Z, Cui Y, Li W. A classification method for complex power quality disturbances using EEMD and rank wavelet SVM. *IEEE Trans Smart Grid*. 2015;6(4):1678-1685. doi:[10.1109/TSG.2015.2397431](https://doi.org/10.1109/TSG.2015.2397431)
- Zhao Y, Li T, Zhang X, Zhang C. Artificial intelligence-based fault detection and diagnosis methods for building energy systems: advantages, challenges and the future. *Renew Sustain Energy Rev*. 2019;109:85-101. doi:[10.1016/j.rser.2019.04.021](https://doi.org/10.1016/j.rser.2019.04.021)
- Wang Z, Wang L, Tan Y, Yuan J. Fault detection based on Bayesian network and missing data imputation for building energy systems. *Appl Therm Eng*. 2021;182:116051. doi:[10.1016/j.applthermaleng.2020.116051](https://doi.org/10.1016/j.applthermaleng.2020.116051)
- Lee CY, Shen YX. Optimal feature selection for power-quality disturbances classification. *IEEE Trans Power Delivery*. 2011;26(4):2342-2351. doi:[10.1109/TPWRD.2011.2149547](https://doi.org/10.1109/TPWRD.2011.2149547)
- Xiao X, Li K. Multi-label classification for power quality disturbances by integrated deep learning. *IEEE Access*. 2021;9: 152250-152260. doi:[10.1109/ACCESS.2021.3124511](https://doi.org/10.1109/ACCESS.2021.3124511)
- Borges FAS, Fernandes RAS, Silva IN, Silva CBS. Feature extraction and power quality disturbances classification using smart meters signals. *IEEE Trans Ind Inform*. 2016;12(2): 824-833. doi:[10.1109/TII.2015.2486379](https://doi.org/10.1109/TII.2015.2486379)
- Beniwal RK, Saini MK, Nayyar A, Qureshi B, Aggarwal A. A critical analysis of methodologies for detection and classification of power quality events in smart grid. *IEEE Access*. 2021;9: 83507-83534. doi:[10.1109/ACCESS.2021.3087016](https://doi.org/10.1109/ACCESS.2021.3087016)
- Hafiz F, Swain A, Naik C, Abecrombie S, Eaton A. Identification of power quality events: selection of optimum base wavelet and machine learning algorithm. *IET Sci Meas Technol*. 2019;13(2):260-271. doi:[10.1049/iet-smt.2018.5044](https://doi.org/10.1049/iet-smt.2018.5044)
- Kanirajan P, Suresh Kumar V. Power quality disturbance detection and classification using wavelet and RBFNN. *Appl Soft Comput*. 2015;35:470-481. doi:[10.1016/j.asoc.2015.05.048](https://doi.org/10.1016/j.asoc.2015.05.048)
- Kaushik R, Mahela OP, Bhatt PK, Khan B, Padmanaban S, Blaabjerg F. A hybrid algorithm for recognition of power quality disturbances. *IEEE Access*. 2020;8:229184-229200. doi:[10.1109/ACCESS.2020.3046425](https://doi.org/10.1109/ACCESS.2020.3046425)
- Dash PK, Prasad ENVDV, Jalli RK, Mishra SP. Multiple power quality disturbances analysis in photovoltaic integrated direct current microgrid using adaptive morphological filter with deep learning algorithm. *Appl Energy*. 2022;309:118454. doi:[10.1016/j.apenergy.2021.118454](https://doi.org/10.1016/j.apenergy.2021.118454)
- Liu Y, Jin T, Mohamed MA, Wang Q. A novel three-step classification approach based on time-dependent spectral features for complex power quality disturbances. *IEEE Trans Instrum Meas*. 2021;70:3000814. doi:[10.1109/TIM.2021.3050187](https://doi.org/10.1109/TIM.2021.3050187)
- Khokhar S, Mohd Zin AA, Memon AP, Mokhtar AS. A new optimal feature selection algorithm for classification of power quality disturbances using discrete wavelet transform and probabilistic neural network. *Measurement*. 2017;95:246-259. doi:[10.1016/j.measurement.2016.10.013](https://doi.org/10.1016/j.measurement.2016.10.013)

18. Ahila R, Sadasivam V, Manimala K. An integrated PSO for parameter determination and feature selection of ELM and its application in classification of power system disturbances. *Appl Soft Comput.* 2015;32:23-37. doi:10.1016/j.asoc.2015.03.036
19. Dash S, Subudhi U. Multiple power quality event detection and classification using a modified S-transform and WOA tuned SVM classifier. *Int J Power Energy Convers.* 2021;12(4): 338-363. doi:10.1504/IJPEC.2021.118050
20. Markovska M, Taskovski D, Kokolanski Z, Dimchev V, Velkovski B. Real-time implementation of optimized power quality events classifier. *IEEE Trans Ind Appl.* 2020;56(4): 3431-3442. doi:10.1109/TIA.2020.2991950
21. Zheng Q, Yang M, Yang J, Zhang Q, Zhang X. Improvement of generalization ability of deep CNN via implicit regularization in two-stage training process. *IEEE Access.* 2018;6: 15844-15869. doi:10.1109/ACCESS.2018.2810849
22. Gong R, Ruan T. A new convolutional network structure for power quality disturbance identification and classification in micro-grids. *IEEE Access.* 2020;8:88801-88814. doi:10.1109/ACCESS.2020.2993202
23. Wang S, Chen H. A novel deep learning method for the classification of power quality disturbances using deep convolutional neural network. *Appl Energy.* 2019;235: 1126-1140. doi:10.1016/j.apenergy.2018.09.160
24. Qiu W, Tang Q, Liu J, Yao W. An automatic identification framework for complex power quality disturbances based on multifusion convolutional neural network. *IEEE Trans Ind Inform.* 2020;16(5):3233-3241. doi:10.1109/TII.2019.2920689
25. Elmaz F, Eyckerman R, Casteels W, Latré S, Hellinckx P. CNN-LSTM architecture for predictive indoor temperature modeling. *Build Environ.* 2021;206:108327. doi:10.1016/j.buildenv.2021.108327
26. Gu D, Gao Y, Li Y, Zhu Y, Wu C. A novel label-guided attention method for multilabel classification of multiple power quality disturbances. *IEEE Trans Ind Inform.* 2022;18(7):4698-4706. doi:10.1109/TII.2021.3115567
27. Li Z, Liu H, Zhao J, Bi T, Yang Q. Fast power system event identification using enhanced LSTM network with renewable energy integration. *IEEE Trans Power Syst.* 2021;36(5): 4492-4502. doi:10.1109/TPWRS.2021.3064250
28. Sindi H, Nour M, Rawa M, Öztürk Ş, Polat K. A novel hybrid deep learning approach including combination of 1D power signals and 2D signal images for power quality disturbance classification. *Expert Syst Appl.* 2021;174:114785. doi:10.1016/j.eswa.2021.114785
29. Li Z, Liu H, Zhao J, Bi T, Yang Q. A power system disturbance classification method robust to PMU data quality issues. *IEEE Trans Ind Inform.* 2022;18:130-142. doi:10.1109/TII.2021.3072397
30. Zheng Q, Yang M, Tian X, Jiang N, Wang D. A full stage data augmentation method in deep convolutional neural network for natural image classification. *Discrete Dyn Nat Soc.* 2020;2020:4706576.
31. Garcia CI, Grasso F, Luchetta A, Piccirilli MC, Paolucci L, Talluri G. A comparison of power quality disturbance detection and classification methods using CNN, LSTM and CNN-LSTM. *Appl Sci.* 2020;10(19):6755.
32. Singh D, Singh B. Investigating the impact of data normalization on classification performance. *Appl Soft Comput.* 2020;97:105524. doi:10.1016/j.asoc.2019.105524
33. Patro SGK, Sahu KK. Normalization: A Preprocessing Stage. 2015.
34. Simonyan K, Zisserman A. Very deep convolutional networks for large-scale image recognition. Paper presented at: 3rd International Conference on Learning Representations. 2015.
35. Neyshabur B, Bhojanapalli S, McAllester D, Srebro N. Exploring generalization in deep learning, Advances in Neural Information Processing Systems. 2017.
36. Mohan N, Soman KP, Vinayakumar R. Deep power: Deep learning architectures for power quality disturbances classification. Paper presented at: 2017 International Conference on Technological Advancements in Power and Energy. 2018. doi:10.1109/TAPENERGY.2017.8397249.

How to cite this article: Cen S, Kim DO, Lim CG. A fused CNN-LSTM model using FFT with application to real-time power quality disturbances recognition. *Energy Sci Eng.* 2023;11:2267-2280. doi:10.1002/ese3.1450